Coupling of the As A_{1g} phonon to magnetism in iron pnictides

N. A. García-Martínez,[1] B. Valenzuela,[1] S. Ciuchi,[2,3] E. Cappelluti,[3,1] M. J. Calderón,[1] and E. Bascones[1]
[1]*Instituto de Ciencia de Materiales de Madrid, ICMM-CSIC, Cantoblanco, E-28049 Madrid, Spain*
[2]*Università dell'Aquila and CNISM, via Vetoio, I-67010 Coppito-L'Aquila, Italy*
[3]*Istituto de Sistemi Complessi, U.O.S. Sapienza, CNR, v. dei Taurini 19, 00185 Roma, Italy*
(Received 26 July 2013; revised manuscript received 19 September 2013; published 4 October 2013)

Charge, spin, and lattice degrees of freedom are strongly entangled in iron superconductors. A neat consequence of this entanglement is the behavior of the A_{1g} As-phonon resonance in the different polarization symmetries of Raman spectroscopy when undergoing the magnetostructural transition. In this work, we show that the observed behavior could be a direct consequence of the coupling of the phonons with the electronic excitations in the anisotropic magnetic state. We discuss this scenario within a five-orbital tight-binding model coupled to phonons via the dependence of the Slater-Koster parameters on the As position. We identify two qualitatively different channels of the electron-phonon interaction: a geometrical one related to the Fe-As-Fe angle α and another one associated with the modification upon As displacement of the Fe-As energy integrals $pd\sigma$ and $pd\pi$. While both mechanisms result in a finite B_{1g} response, the behavior of the phonon intensity in the A_{1g} and B_{1g} Raman polarization geometries is qualitatively different when the coupling is driven by the angle or by the energy integral dependence. We discuss our results in view of the experimental reports.

DOI: 10.1103/PhysRevB.88.165106 PACS number(s): 74.70.Xa, 63.20.kd, 74.25.nd, 74.25.Kc

I. INTRODUCTION

There is ample experimental evidence that iron pnictides present a rich interplay between charge, lattice, and magnetic degrees of freedom. The magnetic transition is commonly accompanied by a structural one. Several phononic spectroscopic signatures show unconventional behavior in the magnetic state.[1–8] At the theoretical level, *ab initio* calculations show that the lattice constants and the phonon frequencies depend sensitively on the presence of magnetism,[9,10] and the comparison with experimental measurements is improved when magnetism is included in the calculations.[9,11–15] Furthermore, the electron-phonon coupling has been shown to be enhanced by magnetism.[10,11,16–20] Within this scenario, the role of the spin degree of freedom in the electron-phonon coupling and its possible relevance in the mechanism of superconductivity has been emphasized in several works.[16,18,21,22]

The electronic and magnetic properties are especially sensitive to the height of the pnictogen atom, which affects the band structure at the Fermi level,[23,24] the magnetic moment,[9,16,21,25–27] and possibly the superconducting critical temperature and gap.[28–31] Accordingly, the A_{1g} As phonon, which involves vibrations of the As atoms along the c axis (see Fig. 1) seems to play a special role. Coupling to this phonon has been detected by ultrafast techniques.[32–35] A rapid development of the magnetic ordering upon the vibrational displacement of the A_{1g} As phonon has been observed.[32] Features in the angle-resolved photoemission spectroscopy (ARPES) spectrum of 11 compounds with an energy scale close to the one of this phonon have been interpreted in terms of polaron formation.[36]

Raman response represents a powerful tool for investigating the properties of lattice dynamics.[1,3,5,8,37–43] A significant narrowing of the A_{1g} As phonon linewidth at the onset of magnetism has been reported, whereas both softening and hardening of the phonon frequency with decreasing temperature have been observed.[1,39,41] Crucial information is also encoded in the intensity of the phonon resonances. In the undistorted paramagnetic state, the A_{1g} As phonon is active neither in the B_{1g} nor in the B_{2g} polarization symmetries. When undergoing the magnetostructural transition, a strong phonon signal emerges in the B_{1g} Raman response but not in B_{2g}.[8,42] In 122 compounds, the A_{1g} intensity shows a strong enhancement in the magnetic state.[1,3,8,42] In spite of this, in $BaFe_2As_2$, the B_{1g} intensity is about 1.5 times larger than the A_{1g} intensity.[8,42] This is not accounted for by the orthorhombic distortion alone, in agreement with the small B_{1g} Raman intensity observed below the nonmagnetic structural transition in FeSe.[44]

The aim of this paper is to analyze the unusual Raman response and the changes on the phonon properties in the magnetic state. We show that the dynamical electron-phonon coupling can be responsible for large and unconventional anomalies in the phonon Raman spectrum. We focus on the out-of-plane As lattice vibrations (the A_{1g} As phonon) for which we explicitly calculate the electron-phonon coupling within the context of a tight-binding Slater-Koster formalism. The electron-phonon coupling is formally split into two main qualitatively different contributions: (i) a purely geometrical one ($\hat{g}^{\alpha}$), related to the variation of the Fe-As-Fe angle α and (ii) a second one ($\hat{g}^{\mathrm{pd}}$) coming from the variation of the Slater-Koster energy integrals $pd\sigma$ and $pd\pi$ (see Ref. 24) upon the modulation of the Fe-As distance. We consider the $(\pi,0)$ magnetic state with magnetic moments ordered antiferromagnetically in the x direction and ferromagnetically in the y direction. Magnetism is included at the mean-field Hartree-Fock level,[45,46] and we study separately its interplay with the sources (i) and (ii) of the electron-phonon interaction. The Raman response is evaluated in the paramagnetic and in the $(\pi,0)$ magnetic states using the proper generalization of the charge-phonon theory[47] discussed in Refs. 48 and 49.

Under generic conditions and excluding any static lattice distortion, the coupling of the phonons with the electronic excitations in the magnetic phase is able by itself to induce a Raman intensity in the B_{1g} Raman polarization. This is

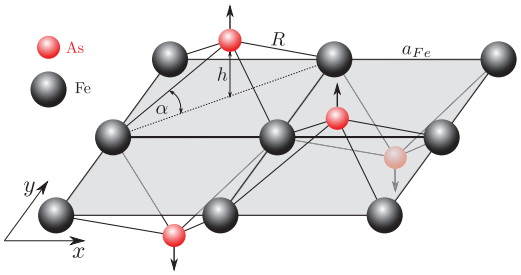

FIG. 1. (Color online) Sketch of the lattice structure showing the A_{1g} As phonon in iron arsenides. The Fe-Fe nearest-neighbor distance a_{Fe}, the Fe-As-Fe angle α, the Fe-As distance R, and the As height with respect to the iron plane h are indicated.

due to the symmetry breaking in the anisotropic magnetic state. Only the electron-phonon coupling $\hat{g}^{\alpha}$ accounts for the fact that the B_{1g} Raman signal can be larger than the A_{1g} Raman signal, the latter strongly decreasing in the magnetic state. A large enhancement in A_{1g} with magnetism appears when coupling electrons and phonons via $\hat{g}^{\mathrm{pd}}$. Based on symmetry considerations, we argue that in the double stripe magnetic order of FeTe the out-of-plane A_{1g} vibrations of the Te atoms will show finite Raman intensity only within the B_{2g} polarization setup and not in the B_{1g} one. With increasing interactions the phonon frequency softens when entering into the magnetic state but hardening is observed for the $\hat{g}^{\mathrm{pd}}$ coupling for the largest values of the on-site electronic interactions U considered.

II. THEORY

A. Model

The Hamiltonian we use to study the electron-phonon coupling on the Fe superconductors has three terms:

$$H = H_0 + H_{\mathrm{ph}} + H_U. \tag{1}$$

H_0 is the five Fe d-orbital tight-binding model for the Fe-As planes, obtained after eliminating the As degree of freedom and previously proposed in Ref. 24. H_{ph} is the phonon part including the free phonon and the electron-phonon interaction, and H_U contains the electronic interactions. The one Fe unit cell is used with x and y directions along the nearest-neighbor Fe-Fe bonds. In the following, we describe in detail each of the terms of the Hamiltonian.

a. Free electron part. The band structure of the system is taken into account via the free electron term H_0,

$$H_0 = \sum_{\mathbf{k},\mu,\nu,\sigma,r} F^r_{\mu\nu}(\mathbf{k}) t^r_{\mu\nu} c^{\dagger}_{\mathbf{k}\mu\sigma} c_{\mathbf{k}\nu\sigma} + \sum_{i,\mu,\sigma} \epsilon_{\mu} c^{\dagger}_{i\mu\sigma} c_{i\mu\sigma}, \tag{2}$$

where $c^{\dagger}_{\mathbf{k}\mu\sigma}$ creates an electron on the Fe d-orbital μ with spin σ and wave vector $\mathbf{k}$, and $c^{\dagger}_{i\mu\sigma}$ represents the same operator in real space. $F^r_{\mu\nu}(\mathbf{k})$ is the electronic $\mathbf{k}$-dispersion relation[24] and ϵ_{μ} is the crystal field. r labels the three different directions for the hoppings $t^r_{\mu\nu}$, with different $\mathbf{k}$ dispersions, taken into account: between first neighbors in the x direction, first neighbors in the y direction, and second neighbors.

Direct Fe-Fe hoppings between their d orbitals and indirect through the As p orbitals are considered. Indirect hopping is included to second order in perturbation theory.[24] Within the Slater-Koster framework considered,[50] the hopping parameters have explicit information on the geometry of the pnictogen tetrahedra. These parameters depend on α, the angle between the Fe-As bond and the Fe plane (see Fig. 1), and on the energy integrals. The direct Fe-Fe hoppings depend on the energy integrals $dd\sigma$, $dd\pi$, and $dd\delta$ between the Fe d orbitals, while the indirect (through the As) Fe-Fe hoppings depend on $pd\sigma$ and $pd\pi$ between the Fe d orbitals and the As p orbitals. These energy integrals are a function of the relative distance between the constituent atoms. The analytic expressions for all the hoppings $t^r_{\mu\nu}$ are given in Ref. 24.

The energy integrals and crystal field ϵ_{μ} parameters in Eq. (2) are chosen to correctly describe the bands, their orbital compositions, the Fermi surface, and the modification induced by α as provided by electronic structure calculations. Details are given in Ref. 24. H_0 has *tetragonal* symmetry, i.e., the static orthorhombic distortion found in the magnetic phase is not included in our calculations.

b. Phonon part. H_{ph} is given by

$$H_{\mathrm{ph}} = \sum_{\mathbf{q}} \omega_{\mathbf{q}} a^{\dagger}_{\mathbf{q}} a_{\mathbf{q}} + \sum_{\mathbf{k},\mathbf{q},\mu,\nu,\sigma,M} g^M_{\mu\nu}(\mathbf{k},\mathbf{q}) c^{\dagger}_{\mathbf{k}+\mathbf{q}\mu\sigma} c_{\mathbf{k}\nu\sigma} (a_{\mathbf{q}} + a^{\dagger}_{-\mathbf{q}}), \tag{3}$$

where $a^{\dagger}_{\mathbf{q}}$ creates a phonon in the A_{1g} As-mode at wave vector $\mathbf{q}$, $\omega_{\mathbf{q}}$ is the phonon frequency and $g^M_{\mu\nu}(\mathbf{k},\mathbf{q})$ the electron-phonon matrix element between orbitals μ and ν. M labels the type of interaction considered. The vertical displacement of the As atoms δh (squeezing and elongating the tetrahedra) gives rise to a modification of α around the equilibrium position α_0 and to a variation of the energy integrals $pd\sigma$ and $pd\pi$ (only the indirect hoppings are affected by this phonon). The two interaction terms that arise are labeled $\hat{g}^{\alpha}$ and $\hat{g}^{\mathrm{pd}}$, namely, $M = \alpha$ and $M = \mathrm{pd}$, respectively. In each of these cases, the electron-phonon interaction may arise from the variation of the hopping $t^r_{\mu\nu}$ with phonon coordinates giving rise to *nonlocal* contributions, and from the variation of the crystal field ϵ_{μ} resulting in *local* contributions: $g^M = g^{M,\mathrm{loc}} + g^{M,\mathrm{nonloc}}$.

The crystal field ϵ_{μ} can be decomposed in a term which includes the electrostatic interactions between the ions in the system $\epsilon^{\mathrm{Coul}}_{\mu}$ and a contribution that depends on the As orbital energies $\epsilon^{\mathrm{ind}}_{\mu}$. The dependence of $\epsilon^{\mathrm{Coul}}_{\mu}$ on the As position is beyond the scope of the present study and is neglected here. We only consider the dependence of $\epsilon^{\mathrm{ind}}_{\mu}$ (see Appendix).

The nonlocal part $\hat{g}^{\alpha,\mathrm{nonloc}}$ involves the derivatives of the hoppings with respect to α [straightforwardly calculated from h, the distance between the As atoms and the Fe plane, and a_{Fe}, the Fe-Fe nearest-neighbor distance, as $\alpha = \arctan(\sqrt{2}h/a_{\mathrm{Fe}})$, see Fig. 1] and a form factor $\tilde{F}^r_{\mu\nu}(\mathbf{k},\mathbf{q})$, which depends on the symmetry of the lattice and the orbitals. As we are here interested in the Raman response, $\mathbf{q} = \mathbf{0}$ and $\tilde{F}^r_{\mu\nu}(\mathbf{k},\mathbf{q}) = F^r_{\mu\nu}(\mathbf{k})$. In the orbital basis, the $\hat{g}^{\alpha,\mathrm{nonloc}}$ electron-phonon coupling is given by

$$g^{\alpha,\mathrm{nonloc}}_{\mu\nu}(\mathbf{k}) = \sum_r F^r_{\mu\nu}(\mathbf{k}) \frac{\partial t^r_{\mu\nu}}{\partial \alpha} \delta\alpha\,, \tag{4}$$

with $\delta\alpha = \frac{\partial\alpha}{\partial h}\delta h$ and form factors $F^r_{\mu\nu}(\mathbf{k})$ as in Eq. (2). Analogously,

$$g^{\alpha,\mathrm{loc}}_{\mu\mu} = \frac{\partial\epsilon^{\mathrm{ind}}_{\mu}}{\partial\alpha}\delta\alpha\,. \tag{5}$$

This contribution to the interaction Hamiltonian appears as a constant (non-$\mathbf{k}$-dependent) diagonal term.

$\hat{g}^{\mathrm{pd}}$ involves the derivatives of the hoppings with respect to $pd\sigma$ and $pd\pi$. These integrals are a decaying function of R, the distance between Fe and As atoms. R is related to h as $R = h/\sin\alpha$. We assume the R dependence is the same for both $pd\sigma$ and $pd\pi$: $pd\sigma = C_{pd\sigma}f(R)$ and $pd\pi = C_{pd\pi}f(R)$. If R_0 is the Fe-As distance corresponding to the equilibrium angle α_0, $pd\sigma_0 = C_{pd\sigma}f(R_0)$ and $pd\pi_0 = C_{pd\pi}f(R_0)$. Expanding around this equilibrium value $pd\sigma = pd\sigma_0[1 + \frac{1}{f(R_0)}\frac{\partial f(R)}{\partial R}\delta R]$, and equivalently for $pd\pi$. Therefore $\delta pd\sigma = pd\sigma_0\frac{1}{f(R_0)}\frac{\partial f(R)}{\partial R}\frac{\partial R}{\partial h}\delta h$ and $\delta pd\pi = pd\pi_0\frac{1}{f(R_0)}\frac{\partial f(R)}{\partial R}\frac{\partial R}{\partial h}\delta h$. Consequently, $\delta pd\pi = \frac{pd\pi_0}{pd\sigma_0}\delta pd\sigma$. Using these relations, in the orbital basis,

$$g^{pd,\mathrm{nonloc}}_{\mu\nu}(\mathbf{k}) = \sum_r F^r_{\mu\nu}(\mathbf{k})\delta pd\sigma\left(\frac{\partial t^r_{\mu\nu}}{\partial pd\sigma} + \frac{\partial t^r_{\mu\nu}}{\partial pd\pi}\frac{pd\pi_0}{pd\sigma_0}\right), \tag{6}$$

$$g^{pd,\mathrm{loc}}_{\mu\mu} = \delta pd\sigma\left(\frac{\partial\epsilon^{\mathrm{ind}}_{\mu}}{\partial pd\sigma} + \frac{\partial\epsilon^{\mathrm{ind}}_{\mu}}{\partial pd\pi}\frac{pd\pi_0}{pd\sigma_0}\right). \tag{7}$$

Here, we take $f(R) = 1/R^4$. This dependence is valid assuming the p and d orbitals are very localized and they only couple through plane-wave corrections to the atomic state wave functions.[51] The pnictides have a strong covalent character that may invalidate the localization assumption, hence this particular functional dependence must be taken with caution. Therefore a direct quantitative comparison between $\hat{g}^{\alpha}$ and $\hat{g}^{\mathrm{pd}}$ would not be reliable, hence we present the results for the two electron-phonon interactions separately.

c. Correlation part. H_U includes the local interactions (intraorbital U, Hund's coupling J_H and interorbital $U' = U - 2J_H$) and is treated within Hartree-Fock mean-field approximation with focus on the $(\pi,0)$ antiferromagnetic state (see Refs. 45 and 46 for details). The Hartree-Fock self-consistency includes the electronic degrees of freedom and not the phonons. The model without phonons $(H_0 + H_U)$ has been previously used to study the magnetic phase diagram as a function of U and J_H/U within a Hartree-Fock approximation.[45,46,52] With increasing U, a metallic AF $(\pi,0)$ state arises. For a narrow range of values of U, the system can be described as itinerant, but a strong orbital differentiation develops for larger values of U.[46] In the orbital differentiated region, the $3z^2 - r^2$, $x^2 - y^2$, and zx orbitals are itinerant, while xy and yz are gapped at half-filling at the Fermi energy. These results are consistent with experimental[53,54] and theoretical[55–58] reports of different renormalization values for the bands depending on their orbital character. In our calculations,[46] for $J_H/U = 0.25$ the itinerant region occurs for $1.45\mathrm{eV} < U < 1.7$ eV and the orbital differentiation for $U > 1.7$ eV.

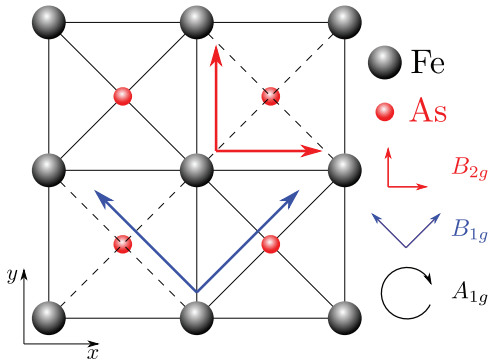

FIG. 2. (Color online) A_{1g}, B_{1g}, and B_{2g} Raman symmetries for the Fe-As layer. We work in the one Fe unit cell with x and y directions along the nearest-neighbor Fe-Fe bonds.

B. Phonon-mediated Raman scattering theory

Raman scattering measures the total cross section of the inelastic scattering of electrons,

$$\frac{\partial^2\sigma}{\partial\Omega\partial\omega_S} = hr_0^2\frac{\omega_S}{\omega_I}S(i\Omega\to\Omega + i0), \tag{8}$$

with ω_I and ω_S the frequency of the incident and the scattered light, respectively, and r_0 the Thomson radius. The Raman intensity can be related to the imaginary part of the Raman response function

$$S^{\lambda}(\Omega) = -\pi^{-1}(1 + n(\Omega,T))\mathrm{Im}\chi^{\lambda}(\Omega) \tag{9}$$

with $\lambda = B_{1g}, B_{2g}, A_{1g}$, the symmetries of the squared lattice point group depending on the incident and scattered photon polarizations represented in Fig. 2. The symmetries are defined with the x and y axes along the Fe-Fe nearest neighbors, as in the Hamiltonian. This definition is different from the one used in some experimental papers.[8]

Only nonresonant diagrams are included in the calculation of the Raman response. To study the phonon contribution, we use the charge-phonon theory originally proposed by M.J. Rice[47] for the optical conductivity and recently used[48,49] to study the Raman response in graphene. The Raman response includes the diagrams shown in Fig. 3: the electronic bubble contribution $\chi^{\lambda}_{\text{el-el}}$ (left) and the charge-phonon diagram $\Delta\chi^{\lambda}_{\mathrm{ph}}$ (right),

$$\chi^{\lambda}(\Omega) = \chi^{\lambda}_{\text{el-el}}(\Omega) + \Delta\chi^{\lambda}_{\mathrm{ph}}(\Omega)\,. \tag{10}$$

The electronic Raman response $\chi^{\lambda}_{\text{el-el}}$ was studied in Ref. 59 and is not discussed in this work. Here, we concentrate our attention on the phonon-mediated Raman response that can be expressed as a sum on all electron-phonon channels

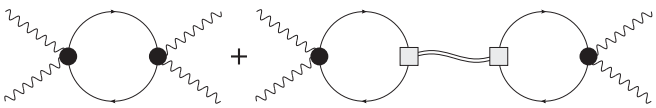

FIG. 3. Electronic Raman (left) and phonon-mediated Raman (right) diagrams. The wavy line is the photon propagator, the double wavy line is the phonon propagator. The circle stands for the Raman vertex and the square for the electron-phonon interaction, either $\hat{g}^{\alpha}$ or $\hat{g}^{\mathrm{pd}}$. The electronic Raman diagram was studied in Ref. 59.

M,M': $\Delta\chi^{\lambda}_{\rm ph}(\Omega)=\sum_{M,M'}\Delta\chi^{\lambda}_{{\rm ph},M,M'}$,

$$\Delta\chi^{\lambda}_{{\rm ph},M,M'}(\Omega)=\chi^{\lambda}_{M}(\Omega)D_0(\Omega)\chi^{*\lambda}_{M'}(\Omega)\,, \tag{11}$$

with $D_0(\Omega)=D_0(\mathbf{q}=0,\Omega)$ the phonon propagator. To address separately the contribution of a single electron-phonon channel, we focus on the diagonal part of $\Delta\chi^{\lambda}_{{\rm ph},M,M'}=\Delta\chi^{\lambda}_{{\rm ph},M}$.

In the vicinity of the resonance, we can approximate

$$D_0(\Omega)=\frac{1}{(\Omega-\Omega_0)+i\Gamma_0} \tag{12}$$

with Ω_0 the phonon frequency and Γ_0 the phonon scattering rate.

χ^{λ}_{M} is a mixed response which includes both the electron-phonon couplings $\hat{g}^{M}$ defined in Eqs. (4)–(7) and the Raman vertex γ^{λ}. The γ^{λ} vertices encode information of the incident and scattered light and the point group symmetry of the squared lattice.[60] In the orbital basis, they are given by[59]

$$\gamma^{B_{1g}}_{\mu\nu}(\mathbf{k})=\frac{\partial^2\epsilon_{\mu\nu}(\mathbf{k})}{\partial k_x^2}-\frac{\partial^2\epsilon_{\mu\nu}(\mathbf{k})}{\partial k_y^2}\,, \tag{13}$$

$$\gamma^{B_{2g}}_{\mu\nu}(\mathbf{k})=\frac{\partial^2\epsilon_{\mu\nu}(\mathbf{k})}{\partial k_x\partial k_y}\,, \tag{14}$$

$$\gamma^{A_{1g}}_{\mu\nu}(\mathbf{k})=\frac{\partial^2\epsilon_{\mu\nu}(\mathbf{k})}{\partial k_x^2}+\frac{\partial^2\epsilon_{\mu\nu}(\mathbf{k})}{\partial k_y^2}\,, \tag{15}$$

with $\epsilon_{\mu\nu}=\sum_r F^r_{\mu\nu}t^r_{\mu\nu}$ [see Eq. (2)]. Separating real and imaginary parts, $\chi^{\lambda}_{M}=\chi'^{\lambda}_{M}+i\chi''^{\lambda}_{M}$,

$$\begin{aligned}\chi'^{\lambda}_{M}(\Omega)=\frac{1}{V}\sum_{\mathbf{k}\sigma nn'}&\gamma^{\lambda}_{nn'}(\mathbf{k})g^{M*}_{nn'}(\mathbf{k})[f(E_n(\mathbf{k}))-f(E_{n'}(\mathbf{k}))]\\&\times\left[\frac{\Omega+E_n(\mathbf{k})-E_{n'}(\mathbf{k})}{(E_n(\mathbf{k})-E_{n'}(\mathbf{k})+\Omega)^2+\eta^2}\right.\\&\left.+\frac{-\Omega+E_n(\mathbf{k})-E_{n'}(\mathbf{k})}{(E_n(\mathbf{k})-E_{n'}(\mathbf{k})-\Omega)^2+\eta^2}\right],\end{aligned} \tag{16}$$

$$\begin{aligned}\chi''^{\lambda}_{M}(\Omega)=-\frac{\pi}{V}\sum_{\mathbf{k}\sigma nn'}&\gamma^{\lambda}_{nn'}(\mathbf{k})g^{M*}_{nn'}(\mathbf{k})[f(E_n(\mathbf{k}))-f(E_{n'}(\mathbf{k}))]\\&\times[\delta(\Omega+E_n(\mathbf{k})-E_{n'}(\mathbf{k}))\\&-\delta(-\Omega+E_n(\mathbf{k})-E_{n'}(\mathbf{k}))],\end{aligned} \tag{17}$$

with δ functions broadened by η. Here, V is the volume, E_n and $E_{n'}$ label the energies of the bands n and n', $f(E)$ is the Fermi function, $g^{M}_{nn'}(\mathbf{k})=\sum_{\mu\nu}a^{*}_{\mu n}(\mathbf{k})g^{M}_{\mu\nu}(\mathbf{k})a_{\nu n'}(\mathbf{k})$, and $\gamma^{\lambda}_{nn'}(\mathbf{k})=\sum_{\mu\nu}a^{*}_{\mu n}(\mathbf{k})\gamma^{\lambda}_{\mu\nu}(\mathbf{k})a_{\nu n'}(\mathbf{k})$ with $a_{\mu n}$ the matrix that rotates between the orbital and the band basis.[59] The matrix elements $g^{M}_{nn'}(\mathbf{k})$ and $\gamma^{\lambda}_{nn'}(\mathbf{k})$ determine whether the phonon is Raman active.

$\Delta\chi^{\lambda}_{{\rm ph},M}(\Omega)$ can be rewritten as a function of the phonon intensity I^{λ}_{M} and the Fano factor q^{λ}_{M} (see Ref. 49):

$$\mathrm{Im}\Delta\chi^{\lambda}_{{\rm ph},M}(\Omega)=-I^{\lambda}_{M}\frac{\left(q^{\lambda}_{M}\right)^2-1+2\left(\frac{\Omega-\Omega_0}{\Gamma_0}\right)q^{\lambda}_{M}}{\left(q^{\lambda}_{M}\right)^2\left[1+\left(\frac{\Omega-\Omega_0}{\Gamma_0}\right)^2\right]} \tag{18}$$

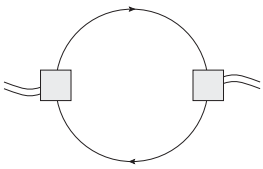

FIG. 4. Phonon self-energy. The square stands for the electron-phonon interaction: either $\hat{g}^{\alpha}$ or $\hat{g}^{\rm pd}$.

with the intensity prefactor I^{λ}_{M} and the Fano factor q^{λ}_{M} given by

$$I^{\lambda}_{M}=\frac{\left[\chi'^{\lambda}_{M}(\Omega_0)\right]^2}{\Gamma_0}\,, \tag{19}$$

$$q^{\lambda}_{M}=-\frac{\chi'^{\lambda}_{M}(\Omega_0)}{\chi''^{\lambda}_{M}(\Omega_0)}\,. \tag{20}$$

This formula will be used below to study the symmetry dependence and intensity of the A_{1g} As phonon. If $|q^{\lambda}_{M}|$ is large, the phonon signal acquires a symmetric shape. If in Eq. (18) we replace $\Omega=\Omega_0$, for $q^{\lambda}_{M}\gg 1$, we find $\mathrm{Im}\Delta\chi^{\lambda}_{{\rm ph},M}(\Omega_0)=-I^{\lambda}_{M}$. The Raman signal turns out positive when replaced in Eq. (9).

C. Phonon self-energy

We study the $\mathbf{q}=0$ phonon self-energy contribution $\Pi_M(\Omega)=\Pi'_M(\Omega)+i\Pi''_M(\Omega)$ arising from the coupling to the electrons. The real part produces a hardening or softening of the phonon and the imaginary part contributes to the phonon broadening. In the second-order perturbation theory approximation,[61] (see Fig. 4) the phonon self-energy can be expressed as a sum on all the electron-phonon channels M,M': $\Pi(\Omega)=\sum_{M,M'}\Pi^{\lambda}_{{\rm ph},M,M'}(\Omega)$. We consider only the diagonal part of the self-energy $\Pi_M(\Omega)$ for which the real and imaginary parts read

$$\begin{aligned}\Pi'_M(\Omega)=\frac{1}{V}\sum_{\mathbf{k}\sigma nn'}&\left|g^{M}_{nn'}(\mathbf{k})\right|^2[f(E_n(\mathbf{k}))-f(E_{n'}(\mathbf{k}))]\\&\times\left[\frac{\Omega+E_n(\mathbf{k})-E_{n'}(\mathbf{k})}{(E_n(\mathbf{k})-E_{n'}(\mathbf{k})+\Omega)^2+\eta^2}\right.\\&\left.+\frac{-\Omega+E_n(\mathbf{k})-E_{n'}(\mathbf{k})}{(E_n(\mathbf{k})-E_{n'}(\mathbf{k})-\Omega)^2+\eta^2}\right],\end{aligned} \tag{21}$$

$$\begin{aligned}\Pi''_M(\Omega)=-\frac{\pi}{V}\sum_{\mathbf{k}\sigma nn'}&\left|g^{M}_{nn'}(\mathbf{k})\right|^2[f(E_n(\mathbf{k}))-f(E_{n'}(\mathbf{k}))]\\&\times[\delta(\Omega+E_n(\mathbf{k})-E_{n'}(\mathbf{k}))\\&-\delta(-\Omega+E_n(\mathbf{k})-E_{n'}(\mathbf{k}))].\end{aligned} \tag{22}$$

A small broadening η, which also enters in the δ functions, has been introduced.

III. RESULTS

We have calculated the phonon contribution to the Raman response and the correction to the phonon self-energy induced by the electron-phonon coupling in the paramagnetic and $(\pi,0)$ antiferromagnetic states at zero temperature. We study the A_{1g} As phonon and consider the two electron-phonon couplings introduced in Sec. II A, $\hat{g}^{\alpha}$ and $\hat{g}^{\rm pd}$. We choose generic interactions to describe the iron pnictides, $J_H=0.25U$

with U ranging from the paramagnetic phase $U < 1.45$ eV, through the itinerant magnetic phase 1.45eV $< U <$ 1.7 eV to the orbital differentiated region[46] $U > 1.7$ eV. $\alpha_0 = 35.3^\circ$ and $n = 6$, corresponding to a regular tetrahedra and undoped pnictides, are considered unless otherwise stated. We take $\delta h = 0.02$ Å, as previously used in the literature,[9,16] and $\Omega_0 = 20$ meV and $\Gamma_0 = 1$ meV for the phonon frequency and scattering rate (values are similar to the experimental ones[1,39,41]). Within the Hartree-Fock approximation used here to include the local interactions, the renormalization of the bands is not properly accounted for. Comparison of *ab initio* electronic structure calculations and ARPES measurements render a factor of 3 for the renormalization of the bands. Therefore once the ground state has been obtained, the energy bands are divided by 3 to account for the renormalization observed in ARPES experiments[62] and not reproduced at the Hartree-Fock level.

A. Raman response

Figure 5 is the main result of this work. It shows the A_{1g} and the B_{1g} phonon Raman intensities due to the couplings $\hat{g}^\alpha$ (left) and $\hat{g}^{\rm pd}$ (right). For both couplings $\hat{g}^M$, the intensity $I_M^{A_{1g}}$ in the A_{1g} polarization is finite in both the paramagnetic and magnetic states while $I_M^{B_{1g}}$ is finite only in the antiferromagnetic state. The B_{2g} phonon intensity, not shown, vanishes in all the range of parameters.[63] While H_0 is tetragonal, this symmetry is broken in the anisotropic $(\pi,0)$ magnetic state. The x and y directions become inequivalent due to the reorganization of the *electronic* degrees of freedom. The B_{1g} signal is antisymmetric under the $k_x \to k_y$ rotation, see Eq. (13), and it is sensitive to k_x being nonequivalent to k_y in the magnetic state. This sensitivity results in a finite $I_M^{B_{1g}}$. B_{2g}, however, is antisymmetric under either $k_x \to -k_x$ or $k_y \to -k_y$, see Eq. (14). $I_M^{B_{2g}}$ is not sensitive to the breaking of the tetragonal symmetry in the $(\pi,0)$ state and remains zero.

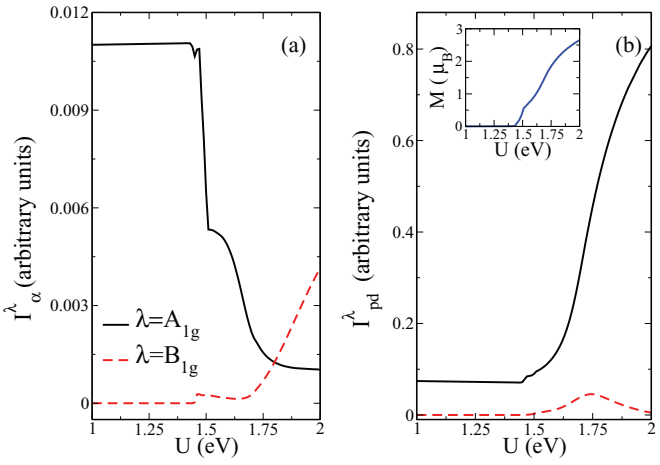

FIG. 5. (Color online) A_{1g} and B_{1g} phonon Raman intensities vs the on-site interaction U for the electron-phonon coupling $\hat{g}^\alpha$ (a) and $\hat{g}^{\rm pd}$ (b). Note that in the magnetic state, $\hat{g}^\alpha$ for $U > 1.8$ eV shows a bigger B_{1g} response than the A_{1g} one, while $\hat{g}^{\rm pd}$ gives a strong enhancement of the A_{1g} polarization signal. Inset in (b) Magnetic moment as a function of the interaction U. $J_H/U = 0.25$, $\Omega_0 =$ 20 meV, $\delta h = 0.02$ Å, $\Gamma_0 = 1$ meV, and $\eta = 3$ meV have been used.

A strong change in the intensity is also observed in the A_{1g} Raman polarization when entering in the magnetic state. The Raman intensity $I_M^{A_{1g}}$ is related to the real part of the mixed bubble at the phonon frequency $\chi_M'^{A_{1g}}(\Omega_0)$ via Eq. (19). $\chi_M'^{A_{1g}}(\Omega_0)$, Kramers-Krönig integral of $\chi_M''^{A_{1g}}(\Omega_0)$, is sensitive to the reorganization of the electronic structure in the magnetic state, especially close to the Fermi level, at energies comparable to Ω_0.

The A_{1g} and the B_{1g} signals show a qualitatively different behavior for the two different electron-phonon couplings considered: $\hat{g}^\alpha$ [see Fig. 5(a)] and $\hat{g}^{\rm pd}$ [see Fig. 5(b)]. In the magnetic state, $I_\alpha^{A_{1g}}$ decreases with respect to the intensity in the paramagnetic state, while $I_{\rm pd}^{A_{1g}}$ increases. $I_\alpha^{B_{1g}}$ increases in the magnetic state while $I_{\rm pd}^{B_{1g}}$ shows a bump as a function of U getting close to zero for $U = 2$ eV.

The nonlocal components of the electron-phonon interactions, Eqs. (4) and (6), appear to dominate the qualitative behavior of the Raman intensity. This can be seen by comparing the total intensities in Fig. 5 with the nonlocal terms of the mixed bubble $\chi_M'^{\lambda}(\Omega_0)$ in Fig. 6 (I_M^λ and $\chi_M'^\lambda$ are

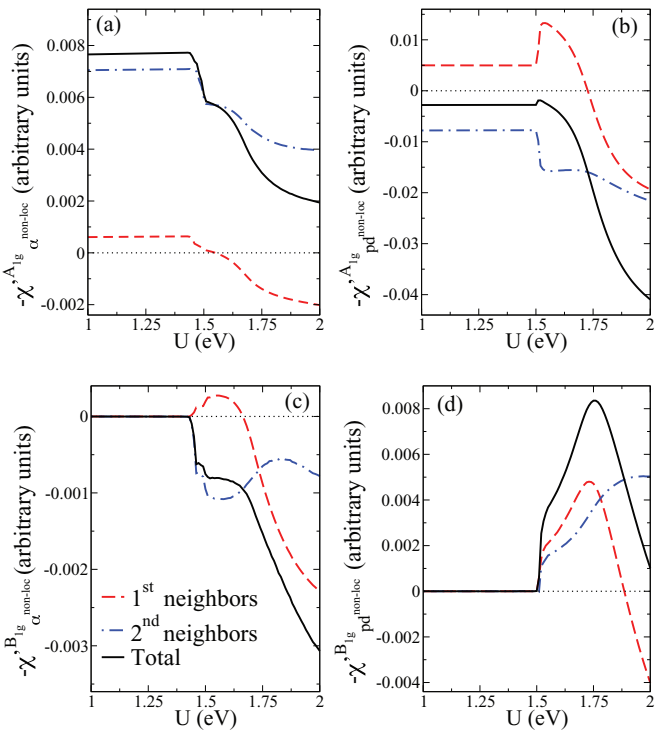

FIG. 6. (Color online) Real part of the nonlocal terms of the mixed bubble $\chi_M'^{\lambda}(\Omega_0)$: $\chi'^{A_{1g}}_{\alpha^{\rm nonloc}}$ (a), $\chi'^{A_{1g}}_{pd^{\rm nonloc}}$ (b), $\chi'^{B_{1g}}_{\alpha^{\rm nonloc}}$(c), and $\chi'^{B_{1g}}_{pd^{\rm nonloc}}$ (d). These nonlocal terms appear to dominate the qualitative behavior of the Raman intensity shown in Fig. 5. (a) First and second nearest-neighbor contributions add up in the paramagnetic state but subtract in the magnetic state while in (b) they almost cancel in the paramagnetic state but add up in the magnetic state. As a result, since I_M^λ is proportional to $\chi_M'^\lambda$ squared, $I_\alpha^{A_{1g}}$ decreases in the magnetic state while $I_{\rm pd}^{A_{1g}}$ increases (see Fig. 5). (d) In the magnetic state, the contributions mostly add up but cancel at high values of U for $\chi'^{B_{1g}}_{pd^{\rm nonloc}}$ which does not happen in (c), explaining the behavior of $I_M^{B_{1g}}$ with U. Same parameters as in Fig. 5.

related by Eq. (19)). The relevant features shown in the solid lines of Fig. 6 mimic the curves in Fig. 5.

The nonlocal components $\chi'^{\lambda}_{M\,\mathrm{nonloc}}(\Omega_0)$ result to be a linear combination of the same **k**-dependent form factors $F^{r}_{\mu\nu}(\mathbf{k})$ in both $M=\alpha$ and $M=pd$ phonon channels. Therefore, for a given photon polarization, the difference in the behavior of χ'^{λ}_{M} and I^{λ}_{M} should be ascribed to the difference in the coefficients of the form factors. In order to gain a deeper insight on this issue, we have further decomposed $\chi'^{\lambda}_{M\,\mathrm{nonloc}}(\Omega_0)$ into first and second nearest-neighbor contributions. In Fig. 6, we see that the different behaviors observed in the Raman intensity in Fig. 5 for the two electron-phonon couplings as a function of U are partly a consequence of the fact that in some cases different contributions add up and in other cases subtract.

The Raman intensities are not just a simple function of the magnetic moment [see inset in Fig. 5(b)]. Nonmonotonic dependencies in momentum are frequently found, especially in the itinerant region. This becomes also clear when comparing the spectrum corresponding to different angles α_0, electron filling n and interactions (not shown). A change in the electron filling and Fe-As-Fe angle induces changes in the band structure and in the transitions at energies close to Ω_0 and, consequently, in the Raman spectrum.

The Fano factors q^{λ}_{M}, not shown, corresponding to $\hat{g}^{\alpha}$ and $\hat{g}^{\mathrm{pd}}$ are calculated using the expression in Eq. (20). For $\hat{g}^{\alpha}$ and for both polarizations B_{1g} and A_{1g}, the Fano factor is generally large and negative with values between -40 and -30 for $U \geqslant 1.8$ eV. For $\hat{g}^{\mathrm{pd}}$ the Fano factor is even larger and still negative reaching around -40 just for $1.8\mathrm{eV} \leqslant U \leqslant 1.9$ eV in the B_{1g} polarization. This Fano factor corresponds to an almost symmetric Lorentzian form of the Raman phonon peak. For smaller values of U, q^{λ}_{M} is strongly dependent on the parameters.

B. Phonon self-energy

Figure 7 shows the contributions of the electron-phonon couplings to the renormalization of the phonon frequency and to the phonon scattering rate as a function of U (see Sec. II C). To better visualize the variations of the phonon frequency and phonon broadening when entering in the magnetic state, we plot $\Delta\Omega_M = \Pi'_M(\Omega_0,U) - \Pi'_M(\Omega_0,U=0)$ in Fig. 7(a) and $\Delta\Gamma_M = \Gamma_M(U) - \Gamma_M(U=0) = -(\Pi''_M(\Omega_0,U) - \Pi''_M(\Omega_0,U=0))$ in Fig. 7(b).

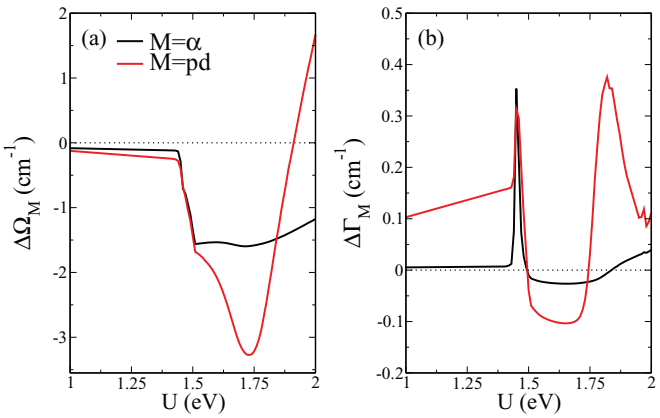

FIG. 7. (Color online) Renormalization of the phonon frequency $\Delta\Omega_M = \Pi'_M(\Omega_0,U) - \Pi'_M(\Omega_0,U=0)$ (a) and phonon broadening $\Delta\Gamma_M = -(\Pi''_M(\Omega_0,U) - \Pi''_M(\Omega_0,U=0))$ (b), for the electron-phonon couplings $\hat{g}^{\alpha}$ and $\hat{g}^{\mathrm{pd}}$. $J_H/U = 0.25$, $\Omega_0 = 20$ meV, $\delta h = 0.02$ Å,[9,16,64] and a δ-function broadening $\eta = 3$ meV have been used.

When entering into the magnetic state ($U \geqslant 1.45$ eV), both $\Delta\Omega_{\alpha}$ (black) and $\Delta\Omega_{\mathrm{pd}}$ (red) are negative, resulting in phonon softening. This nonintuitive behavior is linked to the multiband character of the iron pnictides. Since $\Pi'_M(\Omega)$ is the Kramers-Kronig integral of $\Pi''_M(\Omega)$, the softening is related to the spectral weight redistribution from high energies ($\Omega > \Omega_0$) to lower energies ($\Omega < \Omega_0$) when entering into the magnetic state. In one-band models, when a gap opens, there is a shift of the spectral weight to higher energies and hardening is expected. Due to the multiorbital character of the iron superconductors, the reorganization of the low-energy spectral weight is nontrivial and part of the spectra shifts closer to the Fermi energy, see, for example, Fig. 3 in Ref. 59. $\Delta\Omega_{\alpha}$ is negative in all the range of parameters studied. On the contrary, the nonmonotonic behavior of $\Delta\Omega_{\mathrm{pd}}$ results in hardening for $U > 1.9$ eV. The different behavior due to $\hat{g}^{\mathrm{pd}}$ and $\hat{g}^{\alpha}$ couplings at large values of U is associated with the different way in which the parameters $|g^{M}_{nn'}|^2$ weight the energy excitations around Ω_0 in Eqs. (21) and (22).

As shown in Fig. 7(b), $\Delta\Gamma_{\alpha}$ and $\Delta\Gamma_{\mathrm{pd}}$ as a function of U are nonmonotonic. They change considerably when entering into the magnetic state. Narrowing (broadening) of the phonon linewidth corresponds to negative (positive) $\Delta\Gamma_M$. The large peak at the onset of magnetism at $U = 1.45$ eV is due to a particular band structure reorganization and is not a robust feature for other parameters. For larger interactions, the linewidth shows nonmonotonic behavior: with narrowing followed by broadening.

IV. DISCUSSION AND COMPARISON TO EXPERIMENTS

Here, we discuss our results in comparison with experiment. Note that we address the onset of the magnetic state as a function of the interaction U at zero temperature, while in an experiment the varying parameter is the temperature and the interaction U remains constant. Experimentally, the A_{1g} As phonon appears in the A_{1g} polarization symmetry in the paramagnetic state as a small or nonidentifiable peak,[1,8,42,43] depending on the compound. This peak is strongly enhanced in 122 compounds when decreasing the temperature through the magnetostructural transition.[1,3,8,42] No phonon peak is observed because of symmetry in the B_{1g} polarization geometry in the paramagnetic state whereas a phonon anomaly clearly emerges in the magnetic phase.[8,42,43,65] In $BaFe_2As_2$ the B_{1g} instensity is larger than the one corresponding to the A_{1g} polarization symmetry.[8,42] No peaks are observed in the B_{2g} symmetry in either state. Our calculations reproduce the appearance of a peak in the B_{1g} Raman polarization and not in the B_{2g} one in the anisotropic magnetic state without invoking the structural transition. As discussed in the previous section, this is a consequence of symmetry and not specific to any particular electron-phonon coupling. For the same reason, no Raman signal is obtained in any of these symmetries B_{1g} and B_{2g} in the paramagnetic tetragonal state.

Whereas the appearance or not of an A_{1g} As-phonon peak in the different polarization geometries is quite simple, being dictated by pure group theory arguments, the quantitative discussion of the relative intensities is trickier. Each of the couplings here considered, $\hat{g}^{\alpha}$ and $\hat{g}^{\mathrm{pd}}$, accounts for one of the features observed experimentally but none of them alone can explain both. The coupling via $\hat{g}^{\alpha}$ results, for interactions $U > 1.8$ eV, in a larger intensity in the B_{1g} Raman polarization with respect to the A_{1g} one, as observed experimentally in $BaFe_2As_2$.[8,42] However, this behavior is accompanied by a reduction of the maximum intensity in the A_{1g} polarization symmetry by an order of magnitude in the magnetic state. This is at odds with the strong enhancement of the A_{1g} peak intensity experimentally observed in 122 compounds.[1,3,8,42] An increase of A_{1g} is observed with the coupling $\hat{g}^{\mathrm{pd}}$ but with $I^{A_{1g}} \gg I^{B_{1g}}$.

With the estimated couplings, $\hat{g}^{\mathrm{pd}}$ would dominate the Raman response and $I^{A_{1g}} > I^{B_{1g}}$ would be expected (see Fig. 5). However, as discussed in Sec. II A, the exact dependence of the energy integrals on the As position $f(R)$ is not known. The $1/R^4$ function used is valid for localized orbitals and could strongly overestimate the electron-phonon coupling in a covalent system such as the iron pnictides. A more realistic functional dependence $f(R)$, with a slower dependence on R, or a difference in the distance dependence of $pd\sigma$ and $pd\pi$ could result in a dominance of $\hat{g}^{\alpha}$ with $I^{B_{1g}} > I^{A_{1g}}$. However, note that the relation between magnetization and the system geometry resulting from LDA calculations,[16] with an increase of the magnetization for elongated tetrahedra, would be consistent with a dominance of the pd dependence on the hoppings, while if they are modified according to the α dependence, the magnetization decreases (see Fig. 7 in Ref. 46).

Experimentally,[8] the phonon line shape of undoped compounds has been found to be strongly symmetric with a Fano factor $|q|$ bigger than 30. With electron doping, it acquires an asymmetric shape, with $q \sim -6.5$. The experimental result in undoped pnictides is in agreement with the values of q_M obtained above in the orbital differentiation region. With electron doping we expect to enter into the itinerant region, in which the Fano factor is extremely sensitive to parameters and no robust prediction can be made.

Both hardening and softening of the A_{1g} As phonon have been found in experiments when entering into the magnetic state,[1,39,41] with changes in the phonon frequency of the order of 1–3 cm^{-1} with respect to the zero temperature value. Both electron-phonon coupling and phonon-phonon interaction are expected to contribute to the frequency renormalization, but it is not obvious how to separate the two contributions. Our calculations report softening with frequency renormalizations of the same order of magnitude[64] as experimentally found, except in the case of $\hat{g}^{\mathrm{pd}}$ coupling at large on-site interactions U, which shows hardening.

Raman experiments have also reported a narrowing of the phonon linewidth which, depending on the material, ranges from 1 to 3 cm^{-1} when undergoing a magnetic transition.[1,39,41] For different on-site interactions, our calculations show both narrowing and broadening but with a change in linewidth smaller than observed experimentally.[64] The largest values are associated with the electron-phonon coupling channel $\hat{g}^{\mathrm{pd}}$. The scattering rate is also very sensitive to the broadening parameter η, related to the electron scattering rate, which is reduced in the magnetic state.

Our results show several features compatible with experimental reports but do not offer a completely satisfactory description of the experiments. It is not clear to us whether the discrepancies arise from the approximations done in the calculations (Hartree-Fock description of interactions and magnetism, neglection of the resonant Raman diagrams, lack of a self-consistent treatment of magnetization and phonons on an equal footing, or the coupling constants estimates) or whether electron-phonon couplings beyond those discussed here should be considered. Some of these electron-phonon couplings are (a) the dependence of the Coulombic crystal field $\epsilon_{\mu}^{\mathrm{Coul}}$ on the As position, (b) the dependence of the electronic interaction parameter U on the As position due to the change in the screening[66] or (c) the spin-phonon coupling.[5,21]

V. SUMMARY

In summary, in this paper, we have calculated the Raman spectral properties of the optical out-of-plane As lattice vibrations (the A_{1g} As phonon) in the paramagnetic and in the $(\pi,0)$ magnetic states of the iron pnictides. Using a tight-binding Hamiltonian[24] based on the Slater-Koster approach, we have identified two qualitatively different sources of electron-phonon coupling: one related to the Fe-As-Fe angle α ($\hat{g}^{\alpha}$), and one related to the Fe-As energy integrals $pd\sigma$ and $pd\pi$ ($\hat{g}^{\mathrm{pd}}$). Both of them contain a *local* (**k** independent) and a *nonlocal* (**k** dependent) term, associated with the phonon modulation of the atomic Fe energy levels and with the effective Fe-Fe hopping amplitudes, respectively. The magnetic order has been taken into account by means of a mean-field Hartree-Fock of the electronic Hamiltonian.[45,46] The Raman response of the A_{1g} As phonon has been calculated using a suitable generalization of the charge-phonon theory[47] to the Raman scattering.[48,49]

Our results indicate that a finite Raman intensity can be observed in the magnetic state in the B_{1g} but not in the B_{2g} polarization and it is a consequence of the coupling of the phonons to an anisotropic electronic state with nonequivalent x and y directions. Electron-phonon coupling via $\hat{g}^{\alpha}$ can result in a Raman signal larger in the B_{1g} symmetry than in the A_{1g} symmetry, as observed experimentally in $BaFe_2As_2$. On the other hand, with $\hat{g}^{\alpha}$ coupling the A_{1g} Raman intensity strongly decreases in the magnetic state, contrary to the experimental results. Coupling via $\hat{g}^{\mathrm{pd}}$ produces the opposite behavior: a very large enhancement of the A_{1g} intensity in the magnetic state, which stays much larger than the B_{1g} intensity in all the range of parameters studied. Due to uncertainties in the absolute values of the couplings, it is neither possible to know the intensity resulting from the sum of both $\hat{g}^{\alpha}$ and $\hat{g}^{\mathrm{pd}}$ nor to address careful comparison with experiments.

For most values of the electronic interactions, the electron-phonon coupling induces softening of the phonon frequency in the magnetic state as compared to the paramagnetic state. This behavior is ascribed to the multiorbital character of the iron superconductors. Hardening is observed for large values of the interaction U when coupling happens via $\hat{g}^{\mathrm{pd}}$. Narrowing or

broadening of the phonon line can appear in the magnetic state depending on the parameters.

With symmetry arguments similar to the ones used above, a finite phonon intensity in the B_{1g} symmetry would be also expected in a nematic state[67,68] in the absence of magnetism.[69] We also predict that in the double stripe magnetic state of FeTe, with nonequivalent diagonals, the out-of-plane A_{1g} Te phonon acquires a finite Raman intensity in the B_{2g} polarization geometry, but not in the B_{1g} symmetry. It would be interesting to explore these possibilities experimentally.

ACKNOWLEDGMENTS

We thank Yann Gallais for useful discussions and for sharing unpublished data with us. We have also benefited from conversations with Thomas Frederiksen, Jorge Iñiguez, Lex Kemper, Indranil Paul, and Félix Yndurain. We acknowledge funding from MINECO-Spain through Grants FIS2008-00124, FIS2009-08744, FIS2011-29689, and FIS2012-33521. S.C. acknowledges support from Spanish Education Ministry programme SAB2010-0107. E.C. acknowledges support from the European FP7 Marie Curie project PIEF-GA-2009-251904 and Italian Project PRIN "GRAF" No. 20105ZZTSE.

APPENDIX

The local terms of the electron-phonon couplings $\hat{g}^{\alpha,\mathrm{loc}}$ and $\hat{g}^{\mathrm{pd,loc}}$ are calculated from the derivatives of the crystal field terms $\epsilon_{\mu}^{\mathrm{ind}}$ corresponding to virtual Fe-As forth and back transitions, see Eqs. (5) and (7). The expressions for these terms are calculated to second order in perturbation theory as detailed in Ref. 24 and are given here:

$$\epsilon_{xy,xy}^{\mathrm{ind}} = \frac{1}{|\epsilon_p - \epsilon_d|}\left\{\frac{1}{2}\cos^2\alpha[4pd\pi^2(\cos(2\alpha)-1) - 3pd\sigma^2(\cos(2\alpha)+1)]\right\}, \tag{A1}$$

$$\epsilon_{yz,yz}^{\mathrm{ind}} = \epsilon_{zx,zx}^{\mathrm{ind}} = \frac{1}{|\epsilon_p - \epsilon_d|}\left[pd\pi^2(\cos(2\alpha)-\cos(4\alpha)-2) + \frac{3}{4}pd\sigma^2(\cos(4\alpha)-1)\right], \tag{A2}$$

$$\epsilon_{3z^2-r^2,3z^2-r^2}^{\mathrm{ind}} = \frac{1}{|\epsilon_p - \epsilon_d|}\left[\frac{3}{2}pd\pi^2(\cos(4\alpha)-1) + pd\sigma^2(12\cos(2\alpha)-9\cos(4\alpha)-11)/8\right], \tag{A3}$$

$$\epsilon_{x^2-y^2,x^2-y^2}^{\mathrm{ind}} = \frac{1}{|\epsilon_p - \epsilon_d|}[-4pd\pi^2\cos^2(\alpha)]. \tag{A4}$$

ϵ_p and ϵ_d are the onsite energies for the As p orbitals and for the Fe d orbitals. α is the angle formed by the Fe-As bond and the Fe plane, see Fig. 1. $pd\sigma$ and $pd\pi$ are the energy integrals with values $pd\sigma^2/(\epsilon_d - \epsilon_p) \approx 1$ eV and $pd\pi/pd\sigma = -0.5$, respectively.

[1] K.-Y. Choi, D. Wulferding, P. Lemmens, N. Ni, S. L. Bud'ko, and P. C. Canfield, Phys. Rev. B **78**, 212503 (2008).
[2] M. Le Tacon, T. R. Forrest, C. Rüegg, A. Bosak, A. C. Walters, R. Mittal, H. M. Rønnow, N. D. Zhigadlo, S. Katrych, J. Karpinski *et al.*, Phys. Rev. B **80**, 220504 (2009).
[3] L. Chauviere, Y. Gallais, M. Cazayous, A. Sacuto, M. A. Measson, D. Colson, and A. Forget, Phys. Rev. B **80**, 094504 (2009).
[4] A. Akrap, J. J. Tu, L. J. Li, G. H. Cao, Z. A. Xu, and C. C. Homes, Phys. Rev. B **80**, 180502 (2009).
[5] L. Zhang, P. Guan, D. Feng, X. Chen, S. Xie, and M. Chen, J. Am. Chem. Soc. **132**, 15223 (2010).
[6] A. A. Schafgans, B. C. Pursley, A. D. LaForge, A. S. Sefat, D. Mandrus, and D. N. Basov, Phys. Rev. B **84**, 052501 (2011).
[7] M. Nakajima, T. Liang, S. Ishida, Y. Tomioka, K. Kihou, C. H. Lee, A. Iyo, H. Eisaki, T. Kakeshita, T. Ito *et al.*, Proc. Natl. Acad. Sci. USA **108**, 12238 (2011).
[8] L. Chauvière, Y. Gallais, M. Cazayous, M. A. Méasson, A. Sacuto, D. Colson, and A. Forget, Phys. Rev. B **84**, 104508 (2011).
[9] T. Yildirim, Physica C: Superconductivity **469**, 425 (2009).
[10] L. Boeri, M. Calandra, I. I. Mazin, O. V. Dolgov, and F. Mauri, Phys. Rev. B **82**, 020506 (2010).
[11] M. Zbiri, H. Schober, M. R. Johnson, S. Rols, R. Mittal, Y. Su, M. Rotter, and D. Johrendt, Phys. Rev. B **79**, 064511 (2009).
[12] D. Reznik, K. Lokshin, D. C. Mitchell, D. Parshall, W. Dmowski, D. Lamago, R. Heid, K.-P. Bohnen, A. S. Sefat, M. A. McGuire *et al.*, Phys. Rev. B **80**, 214534 (2009).
[13] S. Hahn, Y. Lee, N. Ni, P. D. Canfield, A. I. Goldman, R. J. McQueeney, B. N. Harmon, A. Alatas, B. N. Leu, E. E. Alp *et al.*, Phys. Rev. B **79**, 220511 (2009).
[14] R. Mittal, M. K. Gupta, S. L. Chaplot, M. Zbiri, S. Rols, H. Schober, Y. Su, T. Brueckel, and T. Wolf, Phys. Rev. B **87**, 184502 (2013).
[15] S. E. Hahn, G. S. Tucker, J.-Q. Yan, A. H. Said, B. M. Leu, R. W. McCallum, E. E. Alp, T. A. Lograsso, R. J. McQueeney, and B. N. Harmon, Phys. Rev. B **87**, 104518 (2013).
[16] F. Yndurain and J. M. Soler, Phys. Rev. B **79**, 134506 (2009).
[17] M. Zbiri, R. Mittal, S. Rols, Y. Su, Y. Xiao, H. Schober, S. Chaplot, M. Johnson, T. Chatterji, Y. Inoue *et al.*, J. Phys.: Condens. Matter **22**, 315701 (2010).
[18] G. Q. Huang, Z. W. Xing, and D. Y. Xing, Phys. Rev. B **82**, 014511 (2010).
[19] B. Li, Z. Xing, and M. Liu, Appl. Phys. Lett. **98**, 072506 (2011).
[20] B. Li, Z. Xing, G. Huang, and M. Liu, J. Appl. Phys. **111**, 033922 (2012).
[21] T. Egami, B. V. Fine, D. Parshall, A. Subedi, and D. J. Singh, Adv. Cond. Matt. Phys. **2010**, 164916 (2010).
[22] C. Gadermaier, V. V. Kabanov, A. S. Alexandrov, L. Stojchevska, T. Mertelj, C. Manzoni, G. Cerullo, N. D. Zhigadlo, J. Karpinski, Y. Q. Cai *et al.*, arXiv:1205.4978.
[23] V. Vildosola, L.Pourovskii, R. Arita, S. Biermann, and A. Georges, Phys. Rev. B **78**, 064518 (2008).
[24] M. J. Calderón, B. Valenzuela, and E. Bascones, Phys. Rev. B **80**, 094531 (2009).

[25]Z. P. Yin, S. Lebègue, M. J. Han, B. P. Neal, S. Y. Savrasov, and W. E. Pickett, Phys. Rev. Lett. **101**, 047001 (2008).
[26]F. Yndurain, Eur. Phys. Lett. **94**, 37001 (2011).
[27]C. de la Cruz, W. Z. Hu, S. Li, Q. Huang, J. W. Lynn, M. A. Green, G. F. Chen, N. L. Wang, H. A. Mook, Q. Si *et al.*, Phys. Rev. Lett. **104**, 017204 (2010).
[28]C. H. Lee, A. Iyo, H. Eisaki, H. Kito, M. T. Fernandez-Diaz, T. Ito, K. Kihou, H. Matsuhata, M. Braden, and K. Yamada, J. Phys. Soc. Jpn. **77**, 083704 (2008).
[29]J. Zhao, Q. Huang, C. de la Cruz, S. Li, J. Lynn, Y. Chen, M. Green, G. Chen, G. Li, Z. Li *et al.*, Nat. Mater. **7**, 953 (2008).
[30]K. Kuroki, H. Usui, S. Onari, R. Arita, and H. Aoki, Phys. Rev. B **79**, 224511 (2009).
[31]G. Garbarino, R. Weht, A. Sow, C. Lacroix, A. Sulpice, M. Mezouar, X. Zhu, F. Han, H. Hu Wen, and M. Núñez Regueiro, Europhys. Lett. **96**, 57002 (2011).
[32]K. W. Kim, A. Pashkin, H. Schfer, M. Beyer, M. Porer, T. Wolf, C. Bernhard, J. Demsar, R. Huber, and A. Leitenstorfer, Nat. Mater. **11**, 497 (2012).
[33]S. Kumar, L. Harnagea, S. Wurmehl, B. Buchner, and A. Sood, Europhys. Lett. **100**, 57007 (2012).
[34]I. Avigo, R. Cortés, L. Rettig, S. Thirupathaiah, H. Jeevan, P. Gegenwart, T. Wolf, M. Ligges, M. Wolf, J. Fink *et al.*, J. Phys.: Condens. Matter **25**, 094003 (2013).
[35]L. Rettig, R. Cortés, J. H.S., P. Gegenwart, T. Wolf, J. Fink, and U. Bovenspiesen, New J. Phys. **15**, 083023 (2013).
[36]Z. K. Liu, R.-H. He, D. H. Lu, M. Yi, Y. L. Chen, M. Hashimoto, R. G. Moore, S.-K. Mo, E. A. Nowadnick, J. Hu *et al.*, Phys. Rev. Lett. **110**, 037003 (2013).
[37]V. G. Hadjiev, M. N. Iliev, K. Sasmal, Y.-Y. Sun, and C. W. Chu, Phys. Rev. B **77**, 220505(R) (2008).
[38]A. P. Litvinchuk, V. G. Hadjiev, M. N. Iliev, B. Lv, A. M. Guloy, and C. W. Chu, Phys. Rev. B **78**, 060503(R) (2008).
[39]Y. Gallais, A. Sacuto, M. Cazayous, P. Cheng, L. Fang, and H. H. Wen, Phys. Rev. B **78**, 132509 (2008).
[40]Y. Zhang, B. Zhou, F. Chen, J. Wei, M. Xu, L. Yang, C. Fang, W. Tsai, G. H. Cao, Z. A. Xu *et al.*, Phys. Rev. B **83**, 054510 (2011).
[41]M. Rahlenbeck, G. L. Sun, D. L. Sun, C. T. Lin, B. Keimer, and C. Ulrich, Phys. Rev. B **80**, 064509 (2009).
[42]S. Sugai, Y. Mizuno, R. Watanabe, T. Kawaguchi, K. Takenaka, H. Ikuta, Y. Takayanagi, N. Hayamizu, and Y. Sone, J. Phys. Soc. Jpn. **81**, 024718 (2012).
[43]A. M. Zhang and Q. M. Zhang, Mod. Phys. Lett. B **26**, 1230020 (2012).
[44]V. Gnezdilov, Y. G. Pashkevich, P. Lemmens, D. Wulferding, T. Shevtsova, A. Gusev, D. Chareev, and A. Vasiliev, Phys. Rev. B **87**, 144508 (2013).
[45]E. Bascones, M. J. Calderón, and B. Valenzuela, Phys. Rev. Lett. **104**, 227201 (2010).
[46]E. Bascones, B. Valenzuela, and M. J. Calderón, Phys. Rev. B **86**, 174508 (2012).
[47]M. J. Rice, Phys. Rev. Lett. **37**, 36 (1976).
[48]E. Cappelluti, L. Benfatto, and A. B. Kuzmenko, Phys. Rev. B **82**, 041402 (2010).
[49]E. Cappelluti, L. Benfatto, M. Manzardo, and A. B. Kuzmenko, Phys. Rev. B **86**, 115439 (2012).
[50]J. Slater and G. Koster, Phys. Rev. **94**, 1498 (1954).
[51]W. Harrison, *Elementary Electronic Structure*, Revised Edition (World Scientific, Singapore, 2004).
[52]M. J. Calderón, G. Leon, B. Valenzuela, and E. Bascones, Phys. Rev. B **86**, 104514 (2012).
[53]T. Yoshida, S. Ideta, I. Nishi, A. Fujimori, M. Yi, R. G. Moore, S. K. Mo, D.-H. Lu, Z.-X. Shen, Z. Hussain *et al.*, arXiv: 1205.6911.
[54]T. Sudayama, Y. Wakisaka, T. Mizokawa, S. Ibuka, R. Morinaga, T. J. Sato, M. Arita, H. Namatame, M. Taniguchi, and N. Saini, J. Phys. Soc. Jpn. **80**, 113707 (2011).
[55]H. Ishida and A. Liebsch, Phys. Rev. B **81**, 054513 (2010).
[56]M. Aichhorn, S. Biermann, T. Miyake, A. Georges, and M. Imada, Phys. Rev. B **82**, 064504 (2010).
[57]Z. P. Yin, K. Haule, and G. Kotliar, Nat. Phys. **7**, 294 (2011).
[58]R. Yu and Q. Si, Phys. Rev. B **86**, 085104 (2012).
[59]B. Valenzuela, M. J. Calderón, G. León, and E. Bascones, Phys. Rev. B **87**, 075136 (2013).
[60]T. Devereaux and R. Hackl, Rev. Mod. Phys. **79**, 175 (2007).
[61]G. D. Mahan, *Many-Particle Physics*, 3rd ed. (Plenum, New York, 2000).
[62]D. H. Lu, M. Yi, S.-K. Mo, A. S. Erickson, J. Analytis, J.-H. Chu, D. J. Singh, Z. Hussain, T. H. Geballe, I. R. Fisher *et al.*, Nature (London) **455**, 81 (2008).
[63]The symmetry of the electron-phonon system determines whether I_M^{λ} is finite or zero. B_{1g} and B_{2g} symmetries are orthogonal to the A_{1g} phonon symmetry in a tetragonal state. As a consequence, $I_M^{B_{1g}}$ and $I_M^{B_{2g}}$ vanish in the paramagnetic state (with tetragonal symmetry).
[64]Both the Raman intensity and the renormalization of the phonon frequency are proportional to $(\delta h)^2$.
[65]S. Sugai, Y. Mizuno, R. Watanabe, T. Kawaguchi, K. Takenaka, H. Ikuta, Y. Takayanagi, N. Hayamizu, and Y. Sone, arXiv:1010.6151.
[66]G. Sawatzky, I. Elfimov, J. van den Brink, and J. Zaanen, Europhys. Lett. **86**, 17006 (2009).
[67]C. Fang, H. Yao, W.-F. Tsai, J. P. Hu, and S. A. Kivelson, Phys. Rev. B **77**, 224509 (2008).
[68]R. M. Fernandes, A. V. Chubukov, J. Knolle, I. Eremin, and J. Schmalian, Phys. Rev. B **85**, 024534 (2012).
[69]A different contribution to the Raman spectrum in a nematic state has been studied in Ref. 70.
[70]H. Yamase and R. Zeyher, arXiv:1306.4267v1.